SVU-International Journal of Engineering Sciences and Applications (2022) 3(2): 11-26
Print ISSN 2785-9967 | Online ISSN 2735-4571
DOI 10.21608/svusrc.2022.137192.1050

# Optimal STATCOM for Performance Improvement of A Grid-Connected PV/Wind Hybrid Energy System: Case Study of Gabal El Zayt Region, Egypt

**Ahmed M. A. Ibrahim[1], I. Hamdan[1], L.S.Nasrat[2], and Mohamed A.Ismeil[1, 3, □]**

**Abstract**: This paper proposes an optimal design of Static Synchronous Compensator (STATCOM) to enhance the dynamic performance of a grid-tied hybrid PV/wind energy system in Gabal El Zayt area situated along the Red Sea coast in Egypt. The design parameters of the STATCOM are optimized by using Particle Swarm Optimization (PSO) algorithm. Moreover, the effectiveness of the optimized STATCOM is validated during real-time changes of the climatic conditions in Gabal El Zayt region as a case study. Also, the credibility of the optimized STATCOM in improving the dynamic operation of the electrical grid is evaluated compared with that of the conventional control strategy during various load scenarios and a three-phase fault occurrence. The obtained results illustrate that the injected power from the hybrid system into the grid is augmented significantly when the optimized STATCOM is employed. Moreover, the optimized STACOM improves substantially the grid voltage and load voltage profile during the load disturbances and the fault incident. Additionally, with the optimized STATCOM support, the dynamic operation of the electrical utility is enhanced considerably by keeping always the grid power factor at unity. `

**Keywords:** PV, wind, hybrid energy system, Static Synchronous Compensator (STATCOM), load, Particle Swarm Optimization (PSO), fault.

## 1 Introduction

Nowadays, the power supply from the traditional energy sources is incapable to satisfy the permanent increase in the power demand of the modern living standards while raising critical environmental issues due to the massive amount of pollutants. Also, with industrialization and urbanization, the electrical utilities have been burdened with the exponential growth of the electricity demand [1]-[2]. Recently, renewable energy sources are utilized for substituting the conventional energy sources and eventually to fulfill the escalating pace of the electricity demand by successfully overcoming the power generation problems. Moreover, the recent trend is merging the distributed power generation sources as hybrid energy systems that have provided a significant improvement to the overall performance of the electrical grids and their reliability. Among all the trending hybrid energy systems, solar PV/wind hybrid power generation system has received great interest worldwide to be integrated with the grid for generating the required power demand with higher continuity and reliability of supply [3]-[4].

In recent decades, several researches have focused on the performance evaluation, energy management, and stabilization enhancement of the grid-tied hybrid energy systems. Among them, Di Wu et al. [5] introduced a modified control strategy including Maximum Power Point Tracking (MPPT) algorithm for extracting the maximum generated power from a grid-connected hybrid PV/wind power system. The obtained results illustrated that the employed MPPT algorithm tracks precisely the peak output power of the hybrid system and improves its dynamic performance effectively under the step variations of the solar irradiance and the wind speed. However, the effectiveness of this MPPT algorithm has not been validated during real-time changes of the climatic conditions. Also, Basaran et al. [6] presented an improved energy management strategy to control the power flow for both standalone and grid-connected PV/wind/battery hybrid energy systems. Although the simulation results proved that the suggested power management scheme boosts the overall efficiency of the system by about 10%, its effectiveness

Received: 7 May 2022/ Accepted: 9 June2022
□Corresponding Author: Mohamed A.Ismeil,
[1]Electrical Engineering Department, Faculty of Engineering, South Valley University, Egypt
[2]Electrical Engineering Department, Faculty of Engineering, Aswan University, Egypt
[3]APEARC, Faculty of Engineering, Aswan University, Egypt

has not been evaluated during variations of linear or non-linear loads.

The main drawbacks of the renewable energy sources are their intermittent nature and the inherent dependence on the climatic conditions which cause significant problems related to the performance stabilization and the generated power quality [7]. Therefore, many studies have suggested the employment of the Flexible AC Transmission Systems (FACTS) devices such as Static Synchronous Compensator (STATCOM) for mitigating the voltage instability and the power quality issues resulting from integrating the hybrid renewable energy systems with the electrical grids [8]. Among them, Jamil et al. [9] discussed the impact of the STATCOM in improving the generated power quality from a grid-connected hybrid PV/wind energy system feeding continuously variable loads. The obtained results illustrated that the employed STATCOM eliminates successfully the disturbance of the generated power under the linear load variations, however, its credibility has not been validated during the fluctuations of the non-linear loads. Kong et al. [10] utilized the STATCOM for regulating the Point of Common Coupling (PCC) voltage of a large-scale PV/wind/battery hybrid power system integrated with the grid. The efficiency of the STATCOM system has been evaluated under practical scenarios of the climatic conditions and the load variations in northeast China. J. Ram et al. [11] utilized the STATCOM to provide reactive power compensation and enhance the PCC voltage stability for a hybrid PV/wind/hydroelectric power system during the occurrence of unbalanced load conditions and transient faults in the electrical grid. Moreover, in [12], the paper proposed an optimal Shunt-Resonance Fault Current Limiter (SRFCL) to improve the transient stability and enhance the Fault Ride-Through (FRT) capability for a grid-tied PV/wind hybrid power system. The efficiency of the proposed SRFCL has been validated during the occurrence of severe symmetrical and unsymmetrical faults in the grid.

On the other hand, Egypt is privileged with renewable energy resources since the abundant solar irradiance and wind especially in Gabal El Zayt region situated along the Red Sea coast. Additionally, Egypt locates in the solar-belt area which is extremely appropriate for implementing large-scale PV projects, where the duration of the irradiance ranges between 9-11 hours/day with an annual average value of 2000-3200 kWh/m$^2$ [13]. Nowadays, several studies have focused on the area of utilizing the PV and wind energy in Egypt. Among them, El-Shimy et al. [14] investigated from the environmental and techno-economical perspectives, the most suitable sites in Egypt for implementing large-scale solar PV plants. This study recommended Wahat Kharga region as the best location to build the large-scale PV stations since it provides the highest energy production and the greatest profitability. Also, Sultan et al. [15] assessed the geographical and environmental conditions of different 27 sites in Egypt for selecting the most appropriate region to build a grid-connected PV station of 100 MW. The paper suggested implementing the PV station project in the area located along the Red Sea coast since it is characterized by an excellent level of solar irradiance. Furthermore, concerning employing the wind energy in Egypt, Hatata et al. [16] evaluated the possibility of harvesting wind power in different locations. This research recommended Gabal El Zayt region for carrying out large-scale wind farms since it is endowed with powerful wind sped.

Additionally, in [17], the paper investigated the role of the STATCOM in augmenting the transient stability performance of a large-scale grid-tied wind power station during the occurrence of a drastic wind gust. F. Tazay et al. [18] proposed implementing a large-scale grid-connected hybrid PV/wind power system of 250 MW in Gabal El Zayt region. The effectiveness of the proposed hybrid system has been validated during real variations of wind speed and irradiance in the study area. Besides, A. Fathy et al. [19] presented an optimum design for a PV/wind/fuel cell hybrid power generation system employed to supply a rural area in Egypt. F. Diab et al. [20] using HOMER software presented an optimum design of a hybrid energy system including PV, wind, battery, and diesel generator to feed a large-scale factory in a remote region. Also, in [21], the paper applied Multi-Objective Genetic Algorithm (MOGA) for determining the optimal size of a grid-connected hybrid energy system supplying residential buildings in New Assiut City, Egypt.

Most previous studies concerning utilizing the renewable energy resources in Egypt have confined to determine the optimum size or optimum location to implement power generation systems connected with the grid. No significant works have been presented to discuss the critical issues such as the generated power quality or fluctuations of the grid voltage due to the occurrence of a sudden fault in the grid or disturbances of the non-linear loads. Motivated by the aforementioned background, this paper proposes an optimal design of STATCOM to enhance the dynamic performance of a grid-connected PV/wind hybrid energy system in Gabal El Zayt region situated along the Red Sea coast in Egypt. The design parameters of the STATCOM are optimized by using Particle Swarm Optimization (PSO) optimization technique. The main contributions of this study can be summarized as follows:

- Proposing an optimal STATCOM to mitigate the grid voltage fluctuations and enhance the hybrid energy system performance during the occurrence of external faults or load disturbances.
- Applying PSO algorithm to obtain the rating power and the control parameters of the STATCOM.
- Utilizing the PV/wind hybrid energy system to feed linear and non-linear loads of a large-scale factory in Gabal El Zayt area.
- Analyzing the dynamic performance of the hybrid energy system during real-time changes of the climatic conditions in Gabal El Zayt region as a case study.
- Validating the effectiveness of the proposed optimized STATCOM compared with that of the conventional control strategy during various load scenarios and a three-phase voltage sag fault occurrence.

## 2 Power System Model Configuration

Fig. 1 shows the schematic of the proposed hybrid energy system and its design specifications are listed in Table 1. It comprises a solar PV plant of 1 MW rating power integrated with a Doubly Fed Induction Generator (DFIG)-based wind power station of 4 MW through the PCC bus. The designed 1 MW PV generation system is consisting of 1000 parallel-connected strings; each string has five PV modules connected in series from Sanyo HIP-200BA3 type with a maximum power of 200.3 W. The technical specifications of the employed PV module are shown in Table 1 and the remaining data are available in [22]. Also, the PV system is equipped with a DC/DC boost converter to implement the MPPT strategy and capture the maximum accessible power during the irradiance changes. On the other hand, the implemented wind station which has a rating power of 4 MW, involves Gamesa G80 wind turbine with the design specifications summarized in Table 1 and the rest of the parameters are available in [23].

The hybrid energy system is utilized to feed local variable loads of a large-scale factory and synchronized with the 220 kV Egyptian community network through a step-up coupling transformer (22/220 kV). Moreover, the STATCOM is employed to improve the system performance and mitigate the PCC voltage disturbances under the load variations especially the non-linear loads or during the grid faults occurrence. In this study, the rating power and the control parameters of the STATCOM have been optimized by using PSO algorithm. In the following sections, the performed control scheme of the hybrid system and the methodology for designing the STATCOM are discussed in detail.

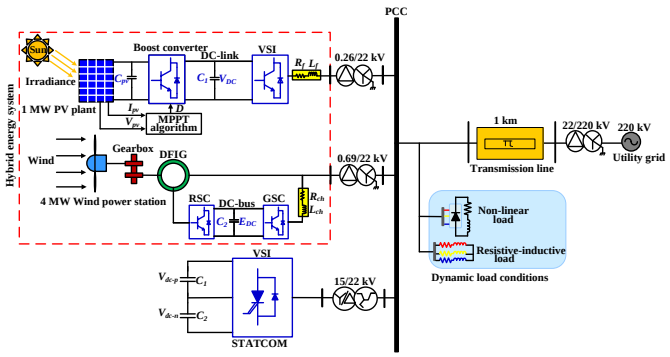


**FIGURE 1. Configuration of the PV/wind hybrid system with STATCOM.**

## 3 The Site under Study

In this work, the dynamic performance of the hybrid system is evaluated during real-time changes of the meteorological conditions in Gabal El Zayt area as a case study. The area under study extends between latitudes 27° 56′and 28° 10′N, and longitudes 33° 30′and 24° 55′ E on the western coast of the Suez Gulf in Egypt [24], as depicted in Fig. 2. The studied region is considered as one of the most encouraging sites to implement renewable energy sources systems given the abundant solar irradiance and wind resources. Fig. 3 illustrates the daily climatic conditions of the irradiance and wind speed in Gabal El Zayt region. These data have been completely gathered from the meteoblue website [25]. The selected site has a good level of irradiation varying from 92.56 W/m$^2$ to 612.3 W/m$^2$ and it is characterized by powerful wind speed ranging between 6.71 m/s and 10.72 m/s.


**FIGURE 1.** Location map of Gabal El Zayt region (site under study) [24].

**TABLE 1. Design specifications of the PV/wind hybrid energy system**

| PV plant | | Wind power station | |
|---|---|---|---|
| **Parameter** | **Value** | **Parameter** | **Value** |
| Rating power | 1 MW | Rating power | 4 MW |
| No. of parallel-connected PV strings | 1000 | Turbine type | Gamesa G80 |
| No. of series-connected modules/string | 5 | Rating power of wind turbine | 2 MW |
| Module type | Sanyo HIP-200BA3 | Cut-in wind speed | 3.5 m/s |
| PV module rating power | 200.32 W | Cut-out wind speed | 25 m/s |
| Solar cells | 96 (monocrystalline) | Rated wind speed | 15 m/s |
| Open-circuit voltage of PV module ($V_{oc}$) | 68.7 V | Rotor diameter | 80 m |
| Short-circuit current of PV moule ($I_{sc}$) | 3.83 A | Swept area | 5027 $m^2$ |
| Module efficiency | 17 % | No. of blades | 3 |
| Module dimensions | 1.3*0.89*0.04 m | Max rotor speed | 1900 rev/min |
| Module weight | 14 kg | Gearbox stages | 3 |
| | | Gearbox ratio | 1:101 |
| **Electrical grid** | | Generator type | DFIG |
| **Parameter** | **Value** | Generator output voltage | 690 V |
| Rated voltage | 220 kV | Frequency | 50 Hz |
| Rated frequency | 50 Hz | Hub height | 78 m |
| S.C level | 1000 MVA | Tower-type | Steel tube |
| X/R | 8 | Tower shape | Conical |

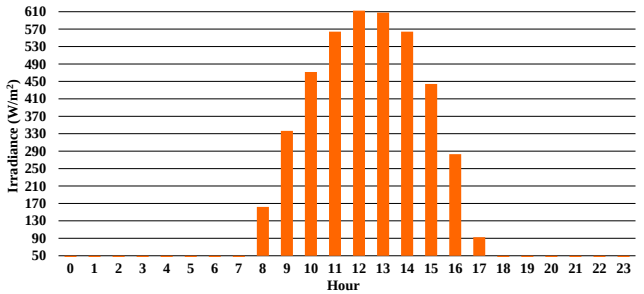


(a) Solar irradiance.

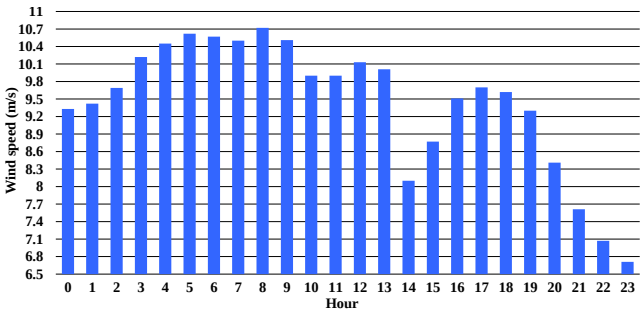


(b) Wind speed.

**FIGURE 3. Real-time climatic conditions in Gabal El Zayt region [25].**

## 4. Control Strategy of the Hybrid Energy System

In this section, the performed control strategy for the PV Voltage Source Inverter (VSI) and also the control scheme of the DFIG are explained in detail.

### 4.1 VSI Control Strategy

The PV plant is synchronized with the common PCC bus via a three-phase, three-level Pulse Width Modulation (PWM) Voltage Source Inverter (VSI). Fig. 4 shows the implemented control strategy of the VSI. The DC-link voltage controller is employed to regulate the voltage of the PV DC-link capacitor ($V_{DC}$) at 1 pu, while the $I_{q\text{-}ref}$ reference current is used to control the generated reactive power from the PV system. During the normal operation conditions, the $I_{q\text{-}ref}$ is determined as zero to sustain the PV plant at the unity power factor. Also, since the output voltage of the VSI must be synchronized with the grid voltage, the grid synchronization is performed by employing the Phase-Locked-Loop (PLL) system, where the angle ($\theta_e$) is extracted to implement the synchronization process [26, 27]. The inner current controller compares the $I_{d\text{-}ref}$ and $I_{q\text{-}ref}$ with the generated active and reactive currents ($I_d$ and $I_q$) to estimate the $V_{d\text{-}VSI\text{-}ref}$ and $V_{q\text{-}VSI\text{-}ref}$ reference voltages of the VSI controller. Finally, the performed control strategy for the VSI can be expressed as [28, 29]:

$$I_{d\_ref} = K_{p\_1}\left(V_{DC\_ref} - V_{DC}\right) + K_{i\_1}\int\left(V_{DC\_ref} - V_{DC}\right)dt \quad (1)$$

$$V_{d\_VSI\_ref} = K_{p\_2}\left(I_{d\_ref} - I_d\right) + K_{i\_2}\int\left(I_{d\_ref} - I_d\right)dt + V_d - \omega_e L_f I_q \quad (2)$$

$$V_{q\_VSI\_ref} = K_{p\_3}\left(I_{q\_ref} - I_q\right) + K_{i\_3}\int\left(I_{q\_ref} - I_q\right)dt + V_q + \omega_e L_f I_d \quad (3)$$

where $V_{DC}$ and $V_{DC\text{-}ref}$ are the voltage of the PV DC-link capacitor and its reference value (1.0 pu), respectively. $K_p$, $K_i$ denote the proportional and integral gains of the PI controller of the VSI, respectively. $\omega_e$ subscribes to the rotation speed of the d-q synchronously reference frame and $L_f$ is the inductance of the PV filter. $V_d$, $V_q$, and $I_d$, $I_q$ represent the d-q axis components of the grid voltage and the generated current by the VSI, respectively.

### 4.2 Rotor Side Converter (RSC) Control Strategy

The RSC is utilized to control the injected active and reactive power from the DFIG stator into the PCC. Fig. 5 describes the control strategy of the RSC. In this control scheme, the DFIG rotor speed controller compares the optimum rotation speed ($\omega_{ref}$) generated by the MPPT technique with the actual rotor speed ($\omega_r$) to provide the reference active current ($I_{dr\text{-}ref}$).

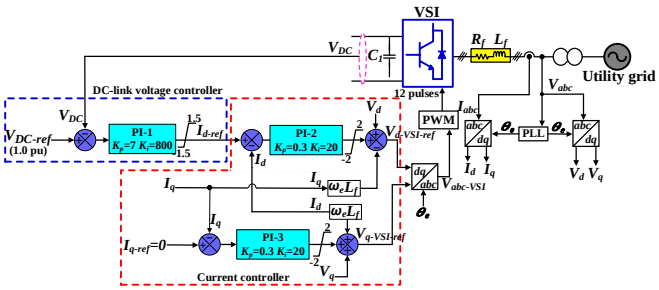


**FIGURE 4. VSI control strategy.**

This reference current is used to track the maximum output power from the wind station under the wind speed changes [30]. On the other hand, the $I_{qr\text{-}ref}$ reference current produced from the VAR regulator loop is employed to adjust the generated reactive power by the DFIG. Under the normal operating conditions, the reactive power reference ($Q_{s\text{-}ref}$) is set as zero to ensure the DFIG operation at the power factor of unity. In other words, the DFIG neither supply nor absorb reactive power to/from the electrical utility. Then, in the inner current control loop, the $I_{dr\text{-}ref}$ and $I_{qr\text{-}ref}$ are compared with the measured rotor currents ($I_{dr}$ and $I_{qr}$) to generate the $V_{dr\text{-}ref}$ and $V_{qr\text{-}ref}$ reference voltages for the RSC controller. This internal current controller is designed to enhance the dynamic response of the control strategy to any disturbance. Finally, the decoupled control strategy of the RSC can be stated as [31, 32]:

$$I_{dr\_ref} = K_{pr1}(\omega_{ref\_}\omega_r) + K_{ir1}\int(\omega_{ref\_}\omega_r)dt \tag{4}$$

$$I_{qr\_ref} = K_{pr3}(Q_{s\_ref} - Q_s) + K_{ir3}\int(Q_{s\_ref} - Q_s)dt \tag{5}$$

$$V_{dr\_ref} = -(\omega_{e\_}\omega_r)\sigma_s L_r I_{qr} + K_{pr2}(I_{dr\_ref} - I_{dr}) + K_{ir2}\int(I_{dr\_ref} - I_{dr})dt \tag{6}$$

$$V_{qr\_ref} = (\omega_{e\_}\omega_r)(\sigma_s L_r I_{dr} + \frac{L_m^2}{L_s} i_{ms}) + K_{pr4}\left(I_{qr\_ref} - I_{qr}\right) + K_{ir4}\int(I_{qr\_ref} - I_{qr})dt \tag{7}$$

Where $\omega_{ref}$, $\omega_r$ are the optimum rotation speed created from the MPPT algorithm and the actual rotation speed of the DFIG rotor, respectively. $Q_s$, $Q_{s\text{-}ref}$ is the generated reactive power from the DFIG stator and its reference value (1.0 pu), respectively. $L_s$, $L_r$ represent the self-inductance of the DFIG stator and rotor windings, respectively and $L_m$ is the magnetizing inductance of the DFIG. $\sigma_s$, $i_{ms}$ are the stator leakage factor and the stator magnetizing current, respectively.

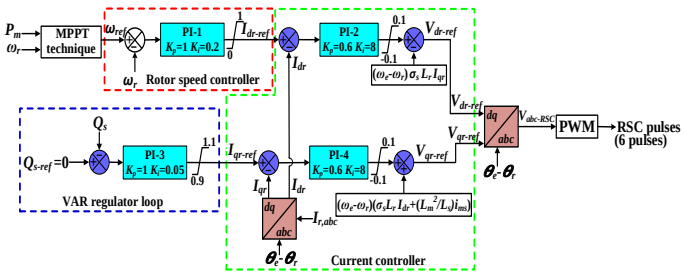


**FIGURE 5. Control strategy of the RSC.**

### 4.3 Grid Side Converter (GSC) Control Strategy

The major objective of the GSC is to maintain the DC-bus voltage between RSC and GSC fixed and it helps to keep a constant power factor for the GSC output. Fig. 6 illustrates the control strategy of the GSC. As shown in the figure, the outer control loop compares the measured DC-bus voltage ($E_{DC}$) with its pre-determined setting (1.0 pu), where the error signal is compensated by a PI controller to output the reference active current ($I_{dg\text{-}ref}$). Additionally, the $I_{qg\text{-}ref}$ reference current is utilized to regulate the exchanged reactive current with the grid. During the normal operation conditions, the $I_{qg\text{-}ref}$ is set at zero to keep the power factor of the GSC output at unity. Then, the inner control loop compares the $I_{dg\text{-}ref}$ and $I_{qg\text{-}ref}$ with the injected GSC currents ($I_{dg}$ and $I_{qg}$) to estimate the $V_{dg\text{-}ref}$ and $V_{qg\text{-}ref}$ reference voltages for the GSC controller. Finally, the decoupled GSC control strategy can be described as follows [33, 34]:

$$I_{dg\_ref} = K_{pg1}\left(E_{DC\_ref} - E_{DC}\right) + K_{ig1}\int\left(E_{DC\_ref} - E_{DC}\right)dt \quad (8)$$

$$V_{dg\_ref} = V_d + \omega_e L_{ch} I_{qg} - K_{pg2}\left(I_{dg\_ref} - I_{dg}\right) - K_{ig2}\int\left(I_{dg\_ref} - I_{dg}\right)dt \quad (9)$$

$$V_{qg\_ref} = -\omega_e L_{ch} I_{dg} - K_{pg3}\left(I_{qg\_ref} - I_{qg}\right) - K_{ig3}\int\left(I_{qg\_ref} - I_{qg}\right)dt \quad (10)$$

Where $k_{pg}$, $k_{ig}$ denote the proportional and integral gains of the PI controller in the GSC control strategy, respectively. $E_{DC}$, $E_{DC\text{-}ref}$ is the voltage of the DFIG DC-bus capacitor and its reference value (1.0 pu), respectively. $L_{ch}$ represents the inductance of the DFIG filter.

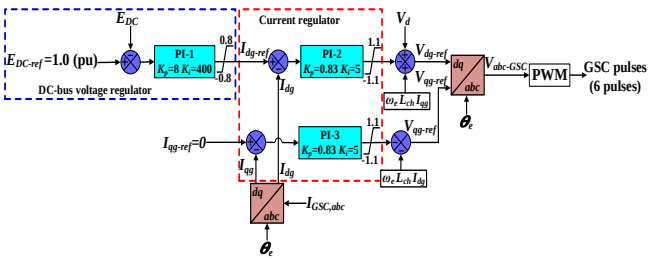


**FIGURE 6. Control strategy of the GSC.**

## 5. Optimal Design of the Static Synchronous Compensator (STATCOM)

In this section, the performed control strategy of the STATCOM system is discussed in detail. Also, the methodology for designing the optimal size and the control parameters of the STATCOM is investigated.

### 5.1 STATCOM Control Strategy

The main objective of the STATCOM system is to suppress the PCC voltage fluctuations during the load variations or fault events by compensating the absorbed reactive power from the grid. Fig. 7 shows the block diagram of the STATCOM controller. In this control scheme, the d-q transformation frame is employed to transform the three-phase PCC voltage and current into their d-q axis components. Also, three optimized PI controllers are mainly used for driving the STATCOM. The PCC voltage regulator provides the quadrature-axis current reference ($I_{qst\text{-}ref}$) to regulate the PCC voltage ($V_{pcc}$) at the rated value (1.0 pu). Then, the current controller compares the injected STATCOM current ($I_{qst}$) with the $I_{qst\text{-}ref}$ reference current to create the required phase shift ($\alpha$) between the generated STATCOM voltage and the grid voltage. Additionally, to eliminate the undesired harmonics of the STATCOM voltage, the DC-link voltage controller keeps the positive and negative voltages of the STATCOM DC-link capacitor equal by applying a slight offset ($\Delta\alpha$) [35]. Finally, the pulses generator unit utilizes the controllers' outputs to generate the switching pulses of the STATCOM's three-level inverter. Therefore, the STATCOM voltage injected into the grid is regulated according to the phase angle ($\alpha$) control. This control strategy for the STATCOM can be described as follows [9]-[36]:

$$I_{qst\_ref} = K_{ps1}\left(V_{pcc\_ref} - V_{pcc}\right) + K_{is1}\int\left(V_{pcc\_ref} - V_{pcc}\right)dt \quad (11)$$

$$\alpha = K_{ps2}\left(I_{qst_{ref}} - I_{qst}\right) + K_{is2}\int\left(I_{qst\_ref} - I_{qst}\right)dt \quad (12)$$

$$\Delta\alpha = K_{ps3}\left(V_{dc_n} - V_{dc_p}\right) + K_{is3}\int\left(V_{dc\_n} - V_{dc\_p}\right)dt \quad (13)$$

Where $V_{pcc}$, $V_{pcc\text{-}ref}$ are the actual PCC voltage and its rated value (1.0 pu), respectively. $V_{dc\text{-}n}$, $V_{dc\text{-}p}$ denote the lower and upper voltage of the STATCOM DC-link capacitor, respectively.

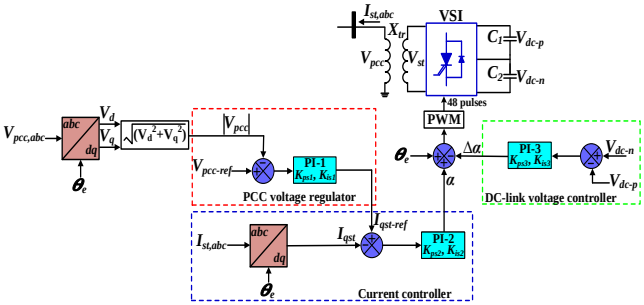


**FIGURE 7. Block diagram of the STATCOM controller.**

### 5.2 Designing of the STATCOM Parameters Using Particle Swarm Optimization (PSO)

The major contribution of this paper is proposing the PSO technique for determining the optimal size and

control parameters of the STATCOM as shown in Table 2. The PSO algorithm is a population-based random search simulating the social behavior of birds, where the main agent is called particle and the group of particles is referred to as population or swarm. Each particle in the swarm is considered as a candidate solution of the optimization problem and it can be represented by the position vector ($X$) and the velocity vector ($V$). The velocity and position of each particle are updated continuously based on its best solution and the global best solution associated with other particles in the swarm, as illustrated in the following equations [37]:

$$V_i^{j+1}=wV_i^j+c_1r_1(Pbest_i^j-X_i^j)+ c_2r_2(Gbest^j-X_i^j) \quad (14)$$

$$X_i^{j+1}= V_i^{j+1}+X_i^j \quad (15)$$

Where $X$, $V$ are the position and velocity of the particles in the swarm, respectively. $i$ denotes the particle number, $j$ is the iteration number, and w is the weight factor used to control the impact of the previous velocity on the current velocity. $r_1$, $r_2$ are uniformly distributed random numbers between [0, 1], $C_1$ is the cognition learning factor, and $C_2$ is the social learning factor. Also, $Pbest_i^j$ denotes the particle's best position and $Gbest^j$ is the global best position found by all particles in the swarm.

Fig. 8 demonstrates the executed PSO flowchart for tuning the optimal size and PI controller parameters of the STATCOM. Also, the convergence curve of the implemented objective function ($O$) is depicted in Fig. 9. The STATCOM parameters listed in Table 2 have been optimized by obtaining the following objective functions:

$$O_{bj1}=Min\ (\Delta V_{pcc}) \quad (16)$$

$$O_{bj2}=Min\ (Q_{grid}) \quad (17)$$

$$O_{bj3}=Max\ (Q_{STATCOM})\ or \quad (18)$$

$$O_{bj3}=Min\ (Q^*_{STATCOM}),\ \text{where}\ Q^*_{STATCOM}=(1/Q_{STATCOM}) \quad (19)$$

$$O=Min(O_{bj1}, O_{bj2}, O_{bj3}) \quad (20)$$

Where *Min*, *Max* denote the minimization and maximization objective functions, respectively. $\Delta V_{pcc}$ represents the fluctuation of the PCC voltage. $Q_{grid}$, $Q_{STATCOM}$ are the injected reactive power from the electrical grid and the STATCOM, respectively.

## 5.3 Power Flow Management System

The major objective of the hybrid energy system is to feed the local variable loads of the factory. These loads can be classified into two types of loads; the first type is the active power loads while the second type represents the reactive power loads. The flow chart of the implemented power flow management strategy for supplying the factory's loads is illustrated in Fig. 10. When the generated active power by the hybrid system exceeds the active power demand of the variable loads, the surplus power will be injected directly into the electrical utility. Otherwise, if the injected power from the hybrid system is insufficient to satisfy the active power demand, the electrical grid provides supplementary support to the loads by supplying the deficit power. On the other hand, the STATCOM is employed to provide the reactive power demand of the loads; however, if the STATCOM is isolated, the reactive power loads are completely fed by the grid. Also, the power flow management system can be expressed as follows:

$$P_{pv} + P_{wind} = P_{load} \pm P_{gird} \quad (21)$$

$$Q_{STATCOM} + Q_{grid} = Q_{load} \quad (22)$$

Where $P_{pv}$, $P_{wind}$ are the generated active power by the PV plant and the wind station, respectively. $P_{load}$ is the required active power of the variable loads and Pgrid denotes the active power absorbed from or injected into the electrical grid. $Q_{grid}$, $Q_{st}$ are the injected reactive power from the grid and the STATCOM, respectively. $Q_{load}$ represents the required reactive power of the loads.

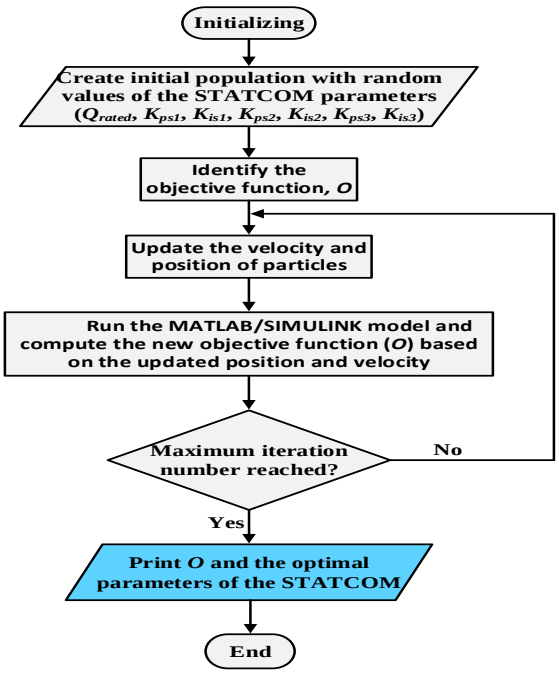


**FIGURE 8. Flowchart for designing the optimal STATCOM parameters using PSO.**

**TABLE 2. Optimal parameters of the STATCOM obtained by PSO algorithm**

| Parameter | Rating power | PCC voltage regulator | | Current controller | | DC-link voltage controller | |
|---|---|---|---|---|---|---|---|
| | | $K_{ps1}$ | $K_{is1}$ | $K_{ps2}$ | $K_{is2}$ | $K_{ps3}$ | $K_{is3}$ |
| **Value** | 150 MVAR | 12.45 | 2834 | 10 | 30.02 | 0.001 | 0.01 |

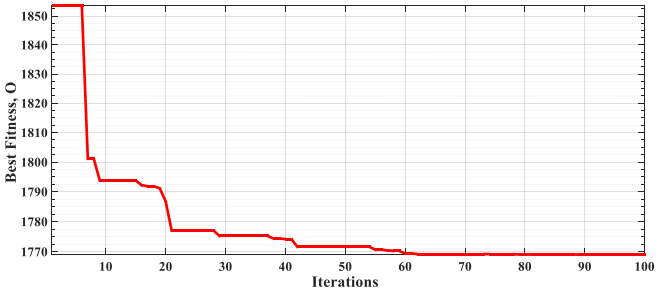


**FIGURE 9. Convergence curve of the objective function.**

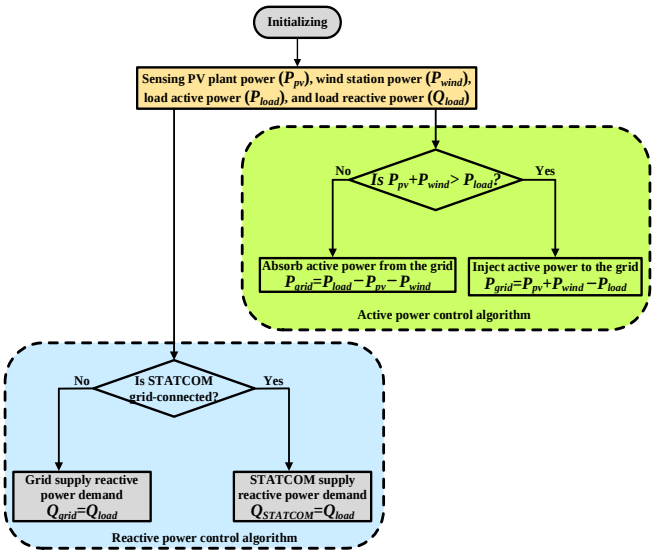


**FIGURE 10. Flow chart of the power flow management system.**

## 6. Simulation Results and Discussions

In this work, the effectiveness of the optimized STATCOM in improving the dynamic performance of the hybrid energy system is evaluated during real-time variations of the climatic conditions in Gabal El Zayt region as a case study. Modeling and simulation of the hybrid system have been implemented using MATLAB/Simulink software. Also, the dynamic response of the optimized control strategy of the STATCOM to the load disturbances is compared with the conventional control system. Moreover, the credibility of the optimized STATCOM in enhancing the operation of the power system and mitigating the PCC voltage fluctuations is validated during various load scenarios and external faults occurrence. This section is divided into four parts:

1) Impact of the optimized STATCOM on the hybrid system performance
2) Dynamic response of the STATCOM control strategy
3) Impact of the optimized STATCOM on the grid operation during load disturbances
4) Impact of the optimized STATCOM on the power system during fault occurrence

### 6.1 Impact of the optimized STATCOM on the hybrid system performance

In this subsection, the role of the optimized STATCOM control strategy in enhancing the dynamic behavior of the hybrid energy system is investigated. The hybrid system performance is analyzed during real changes in solar irradiance and wind speed as a case study of the actual climatic conditions in Gabal El Zayt area. Fig. 11 (a) shows the daily solar irradiance in the study region. The irradiance level rises from 161.9 W/m$^2$ at 8 a.m to the peak value of 612.3 W/m$^2$ at noon, then it decreases gradually until reaching the minimum value of 92.6 W/m$^2$ at 5 p.m. Fig. 11 (b) depicts the generated active power by the PV plant. It is noticed that the PV plant power is augmented significantly when the optimized STATCOM is employed. Therefore, with the STATCOM support, the generated power increases considerably from 125 kW to 581 kW during the morning hours, then it reduces gradually until reaching 62.93 kW at 5 p.m. Also, Table 3 presents a comparison between the generated power from the PV plant power when the optimized STATCOM is utilized and the case when the STATCOM is disconnected. On the other hand, Fig. 11 (c) presents the daily wind speed. It ranges from 6.7 m/s to 10.7 m/s with an average value of 9.45 m/s. Fig. 11 (d) illustrates the generated power from the wind station in response to the wind speed variations. The wind station power grows substantially from 2.15 MW to 3.2 MW during the period between 12 a.m and 8 a.m then fluctuating greatly until reaching its minimum value of 1.1 MW at 11 p.m. Also, Fig. 11 (e) shows the overall injected power from the hybrid system into the PCC. When the optimized STATCOM is utilized, the injected power improves significantly by about 5.67%, where it increases from 2.15 MW at midnight to the maximum value of 3.4 MW at 9 a.m then decreases gradually until reaching 1.1 MW at 11 p.m.

In the following, the implemented control strategy for

the hybrid energy system is validated. Fig. 12 (a) illustrates that the DC-link voltage controller of the VSI keeps successfully the voltage of the PV DC-link capacitor ($V_{DC}$) constant at 1 pu irrespective of the irradiance changes. Fig. 12 (b) shows the dynamic response of the inner current controller of the VSI. It is obvious that the generated active current ($I_d$) follows continuously the Id-ref that varies according to the irradiance level for extracting the maximum generated power by the PV plant. Besides, the generated reactive current ($I_q$) coincides with the $I_{q\text{-}ref}$ at zero to sustain the plant operation at the unity power factor. Similarly, Fig. 12 (c) shows that the d-axis rotor current ($I_{dr}$) tracks the $I_{dr\text{-}ref}$ for obtaining the maximum wind station power, while the q-axis rotor current ($I_{qr}$) coincides with its reference to ensure the DFIG operation at the power factor of unity. Also, Fig. 12 (d) demonstrates that the outer control loop of the GSC maintains effectively the DFIG DC-bus voltage ($E_{DC}$) fixed at 1 pu regardless of the wind speed variations. Additionally, as depicted in Fig. 12 (e), the injected GSC current ($I_{qg}$) remains perfectly at zero for keeping the power factor of the GSC output at unity.

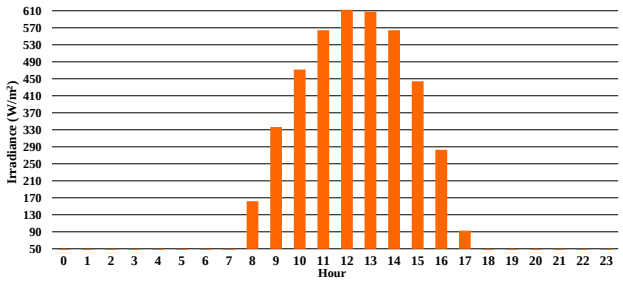


(a) Solar irradiance (case study in Gabal El Zayt area).

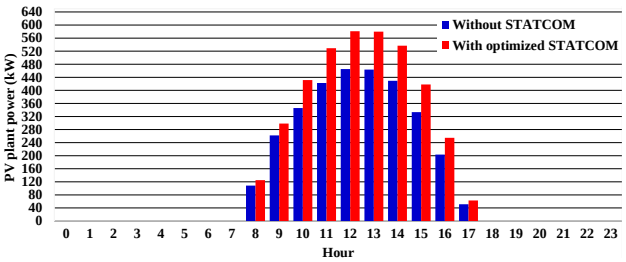


(b) Generated active power by the PV plant.

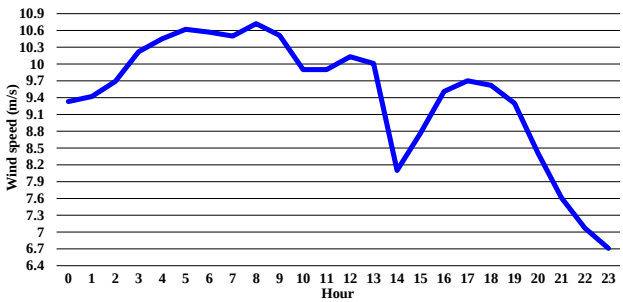


(c) Wind speed (case study in Gabal El Zayt area).

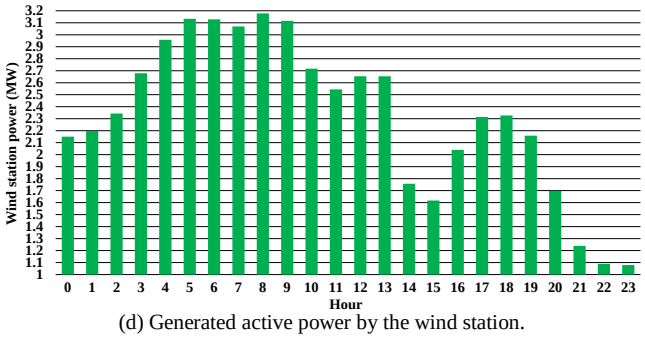


(d) Generated active power by the wind station.

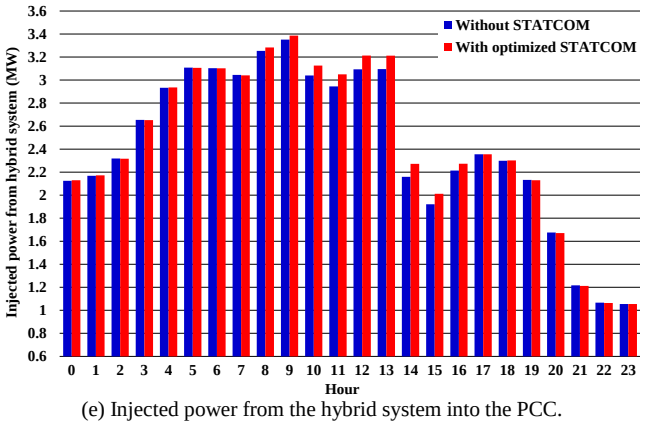


(e) Injected power from the hybrid system into the PCC.

**FIGURE 11. Impact of the optimized STATCOM on the hybrid system performance.**

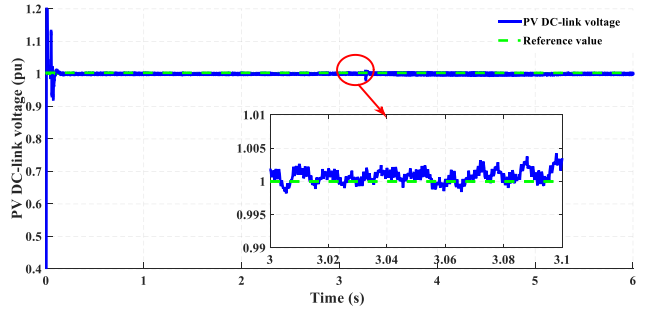


(a) PV DC-link voltage ($V_{DC}$).

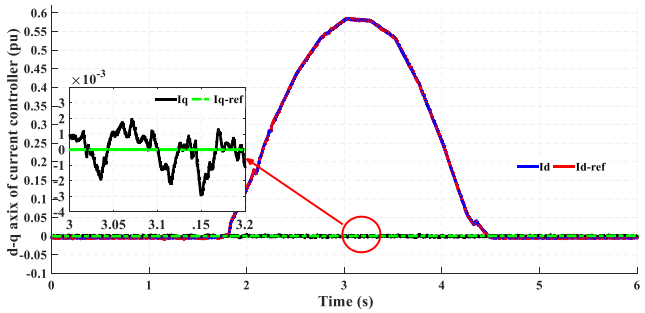


(b) Current controller of the VSI.

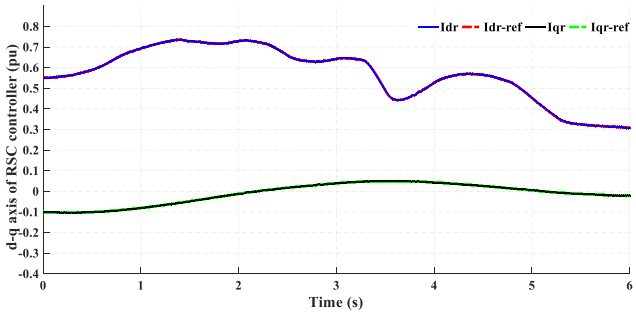


(c) Current controller of the VSI.

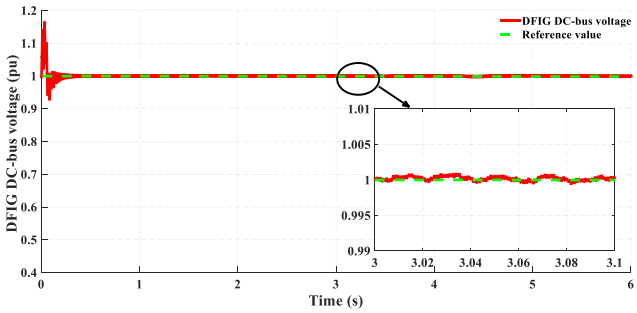


(d) DFIG DC-bus voltage ($E_{DC}$).

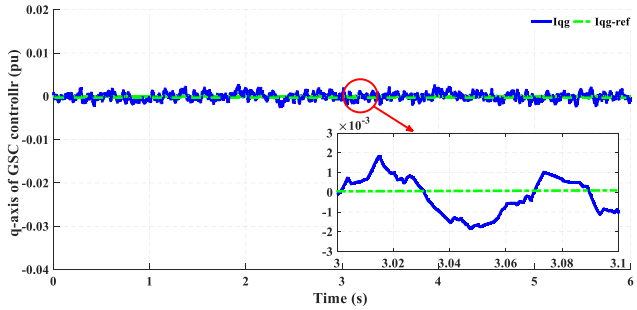


(e) Current regulator of the GSC.

**FIGURE 12. Response of the hybrid system control strategy.**

## 6.2 Dynamic response of the STATCOM control strategy

In this subsection, the dynamic response of the optimized control strategy of the STATCOM to the load disturbances is compared with the conventional control scheme. Fig. 13 shows that the generated STATCOM voltage is less overshot with the optimized control strategy compared with the conventional control scheme. Fig. 14 shows that the injected reactive power by the optimized STATCOM control strategy to supply the loads is less fluctuated compared to the conventional control system. Also, the overshoot of the injected reactive power by the STATCOM is reduced by about 14.91% with the optimized control strategy.

Moreover, Fig. 15 (a) shows that the optimized STATCOM system works in a capacitive operation mode during the inductive loading conditions, where the STATCOM current leads the generated voltage by 90° to provide the required reactive power. Fig. 15 (b) illustrates that the injected STATCOM reactive current ($I_{qst}$) follows accurately its reference ($I_{qst\text{-}ref}$) that varies dynamically to satisfy the absorbed reactive power by the variable loads. Also, it can be noticed that with the optimized control strategy, the overshoots of the STATCOM current are minimized compared with the conventional control system where the design parameters are obtained by trial and error. Fig. 15 (c) demonstrates that the DC-link voltage controller keeps the DC-link voltage of the STATCOM constant to cancel the undesired harmonics of the STATCOM generated voltage. Fig. 15 (d) depicts the reference phase shift ($\alpha$) between the STATCOM voltage and the grid voltage required to supply the reactive power demand.

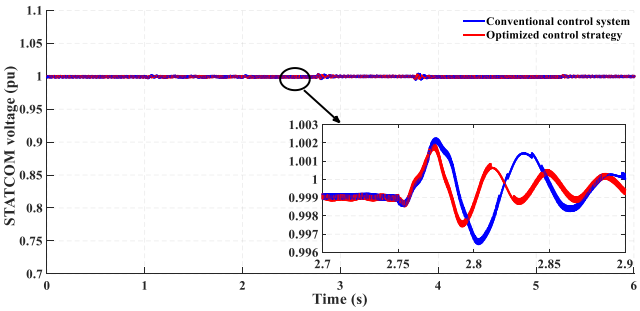


**FIGURE 13. Generated STATCOM voltage.**

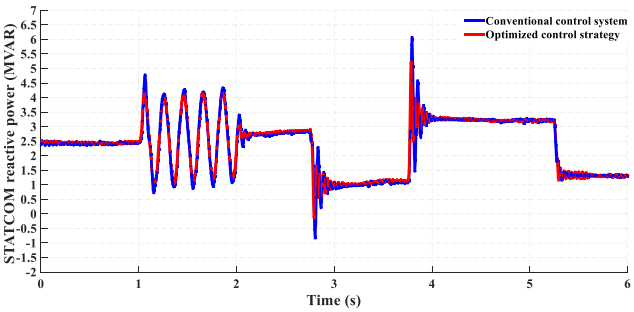


**FIGURE 14. Injected reactive power by the STATCOM.**

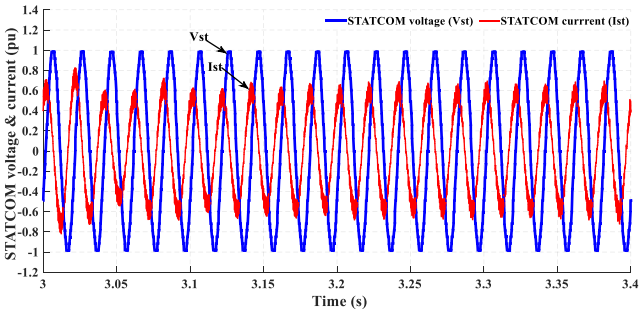


**(a) Generated voltage and current from the STATCOM.**

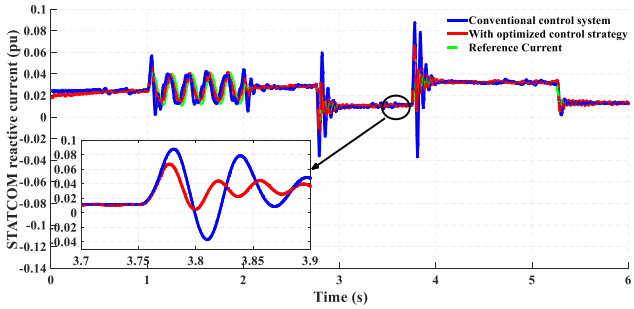


(b) Injected STATCOM reactive current.

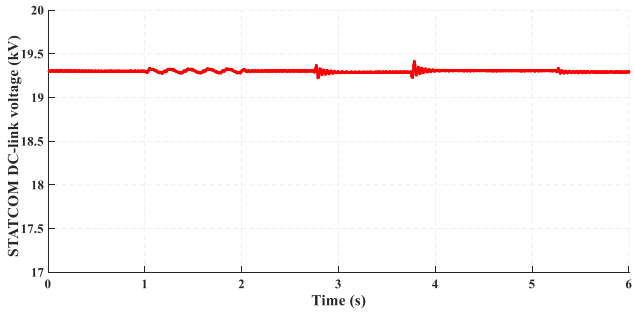


(c) STATCOM DC-link voltage.

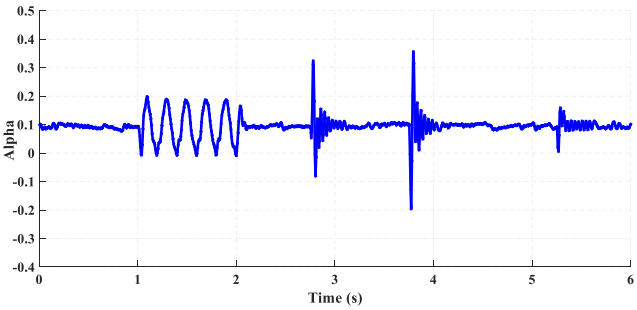


(d) Reference phase shift between the STATCOM voltage and the grid voltage (α).

FIGURE 15. Dynamic response of the STATCOM control strategy.

## 6.3 Impact of the optimized statcom on the grid operation during load disturbances

In the following, the effect of the optimized STATCOM on the dynamic operation of the electrical grid is discussed under load variations. Table 4 illustrates the various load scenarios and the switching time of each load. Also, the absorbed active and reactive power by the variable loads are shown in Fig. 16 (a) and Fig. 16 (b), respectively. It can be noticed that the delivered active and reactive power fluctuate severely during the non-linear loads. Moreover, it can be observed from Fig. 16 (c) that without the optimized STATCOM, the load voltage drops dramatically on the introduction of the inductive loads and oscillates sharply during the non-linear loads. However, with the optimized STATCOM, the voltage profile is improved considerably around its rated value (1 pu).

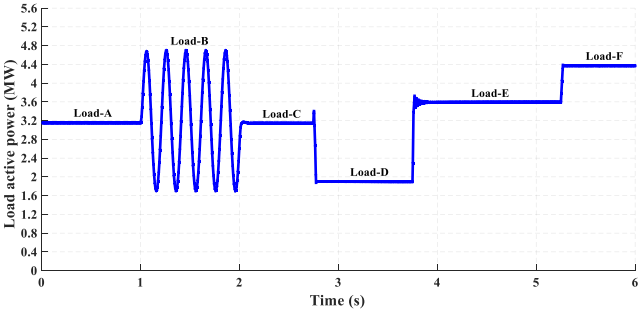


(a) Absorbed active power by the variable loads.

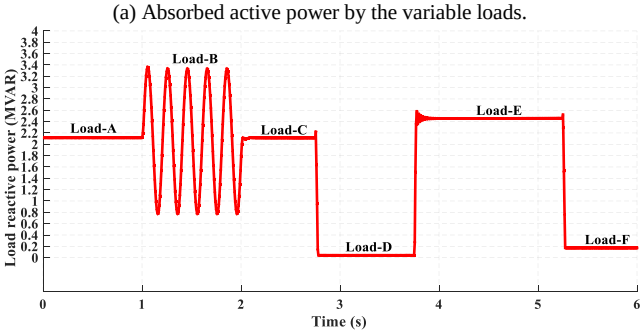


(b) Absorbed reactive power by the variable loads.

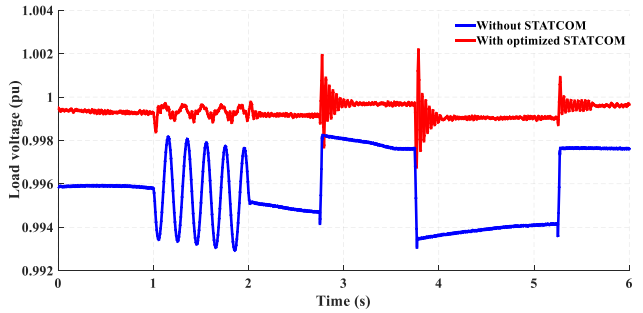


(c) Load voltage.

FIGURE 16. Load variations.

Fig. 17 (a) validates the employed power flow management system between the hybrid system and the variable loads. During the loads-A, C, E, and F, the injected active power from the hybrid system shown in Fig. 11 (e) is greater than the absorbed power by the loads depicted in Fig. 16 (a), so the surplus power is injected into the grid. On the other hand, during the loads B and D, the injected power from the hybrid system is insufficient for achieving the active power demand, thus the grid provides supplementary support by supplying the deficit power. Fig. 17 (b) illustrates the role of the optimized STATCOM in enhancing the dynamic operation of the electrical grid. Without the STATCOM support, the reactive power demand is completely fed by the grid. From the grid code perspective, it is necessary to minimize the injected reactive power by the grid to support its performance and improve the generated power quality. As shown in

the figure, when the optimized STATCOM is utilized to supply the reactive power demand, the injected reactive power from the grid is kept nearly zero despite its oscillations after loads C and D disconnection.

Furthermore, Fig. 17 (c) shows that when the STATCOM system is disconnected, the PCC voltage drops severely especially during the non-linear loads due to the excessive reactive power absorbed from the grid. However, when the optimized STATCOM is employed, the oscillations of the PCC voltage are mitigated significantly that remains near the rated value (1 pu). Also, the role of the STATCOM compensation in improving the power factor of the electrical utility is demonstrated in the following figures. Fig. 17 (d) shows that without the STATCOM support, the phase angle between the injected current and the grid voltage deviates from $0^o$ as an indication of poor power factor. On the other hand, the optimized STATCOM improves the power factor of the electrical utility to be unity where the injected current is in phase with the grid voltage, as illustrated in Fig. 17 (e).

### 6.4 Impact of the optimized statcom on the power system during fault occurrence

In this subsection, the impact of the optimized STATCOM on the dynamic behavior of the power system is analyzed under the occurrence of a three-phase voltage sag fault in the grid. The sag depth is 50% of the grid voltage (i.e. PCC voltage drops to 0.5 pu) occurs at t=3 s and lasts for 150 ms [38]. Fig. 18 (a) shows the effect of the fault on the PCC voltage. It is obvious that without the optimized STATCOM, the PCC voltage falls significantly to 0.5 pu during the fault occurrence. However, when the optimized STATCOM is employed, the voltage improves substantially to 0.67 pu (enhanced by 34%) during the fault while it overshoots to 1.14 pu after fault clearance. Fig. 18 (b) depicts the injected active power from the PV plant. It can be noticed that when the STATCOM is disconnected, the PV power decreases considerably to 0.79 MW when the voltages sag occurs and overshoots sharply to 1.43 MW after fault clearance. However, with the optimized STATCOM, the PV plant continues to inject its rating power of 1 MW during the sag occurrence and the overshoot is eliminated after the fault clearance. Also, Fig 18. (c) shows that when the optimized STATCOM is utilized, the generated power by the wind station is 2.86 MW compared to only 2.19 MW without the STATCOM. Besides, Fig. 18 (d) shows the injected active power from the hybrid system into the grid. Without the optimized STATCOM, the injected power declines severely to 2.98 MW during the fault occurrence. However, when the optimized STATCOM is utilized, the generated power by the hybrid system improves considerably to 3.83 MW (increased by 28.61%).

Furthermore, the impact of the optimized STATCOM on the absorbed active and reactive power by the variable loads are illustrated in Fig. 19 (a) and Fig. 19 (b), respectively. It can be noticed that when the STATCOM is disconnected, the delivered active power to the loads decreases to 0.74 MW, while it improves significantly to 1.32 MW with the optimized

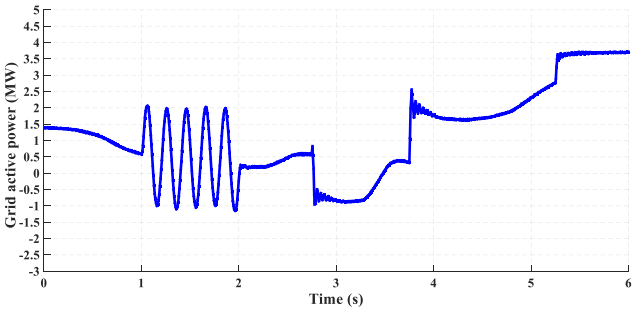


(a) Injected/absorbed active power from the grid.

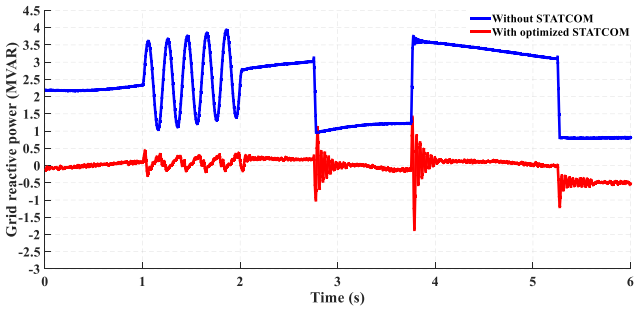


(b) Injected reactive power from the grid.

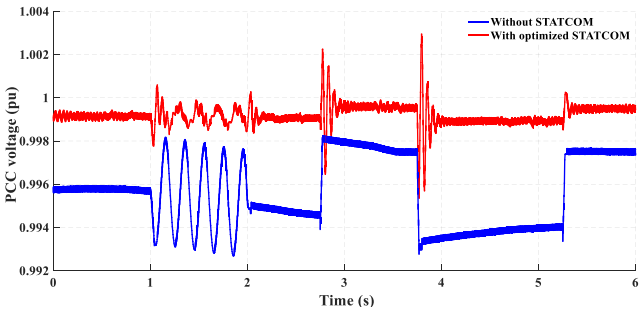


(c) PCC voltage.

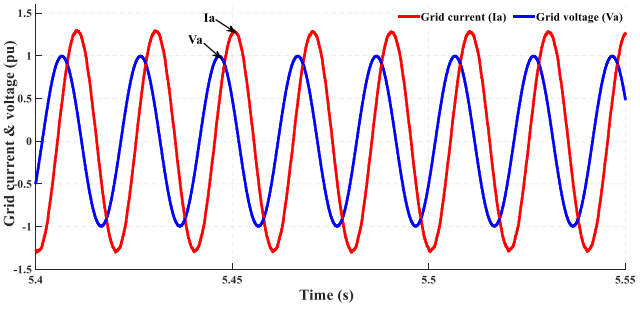


(d) Grid current and grid voltage without optimized STATCOM.

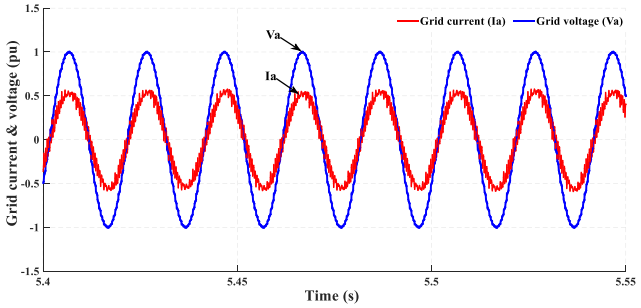


(e) Grid current and grid voltage with optimized STATCOM.

**FIGURE 17. Impact of the optimized STATCOM on the grid operation during load disturbances.**

STATCOM. On the other hand, the absorbed reactive power by the loads reaches 1.5 MVAR when the optimized STATCOM is employed compared to only 0.84 MVAR without the STATCOM. Also, Table 5 summarizes the effect of the optimized STATCOM on the power system under the fault occurrence.

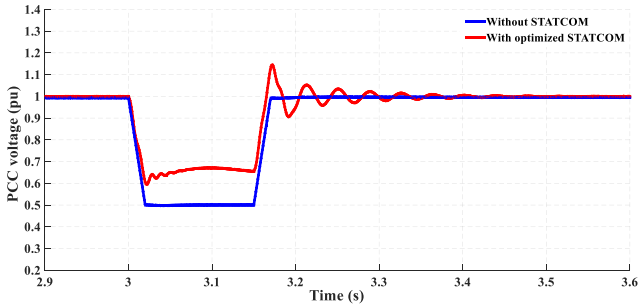


(a) PCC voltage.

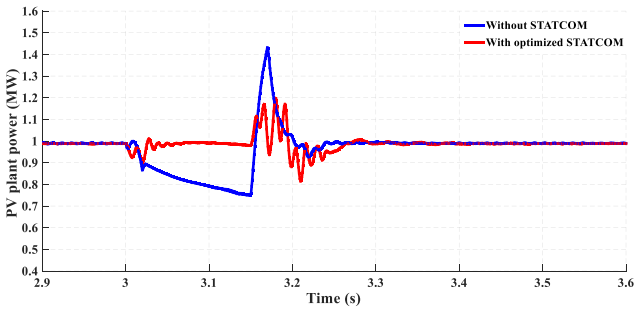


(b) Generated active power by the PV plant.

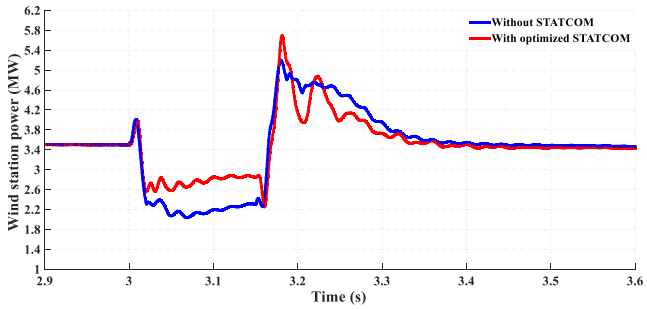


(c) Generated active power by the wind station.

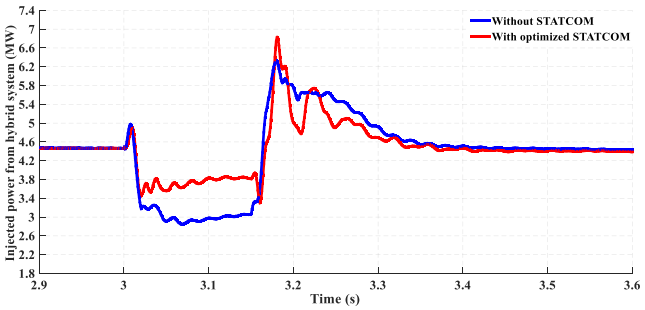


(d) Injected power from the hybrid system.

**FIGURE 18. Impact of the optimized STATCOM on the hybrid system during fault occurrence.**

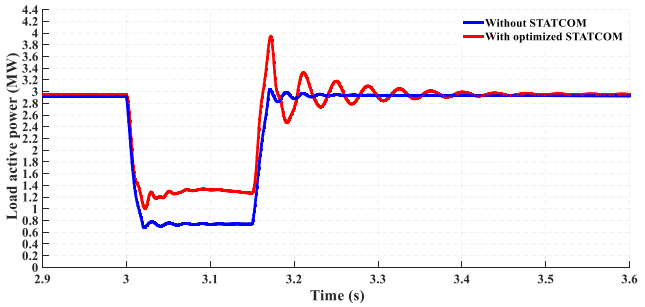


(a) Absorbed active power by the variable loads.

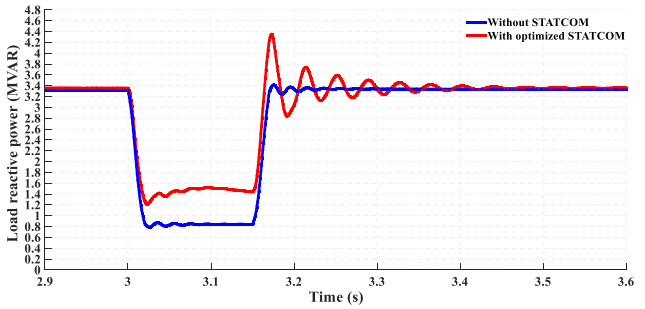


(b) Absorbed reactive power by the variable loads.

**FIGURE 19. Impact of the optimized STATCOM on the load during fault occurrence.**

## 7. Conclusion

This paper proposed an optimal design of STATCOM to enhance the dynamic performance of a grid-connected PV/wind hybrid power system in Gabal El Zayt area region located along the Red Sea coast in Egypt. The rating power and control parameters of the STATCOM are optimized by using the PSO algorithm. Also, the hybrid power system is utilized to feed linear and non-linear loads of a large-scale factory in Gabal El Zayt area. The impact of the optimized STATCOM on the dynamic behavior of the hybrid system is analyzed during actual variations of the climatic conditions in Gabal El Zayt area as a case study. Moreover, the role of

**TABLE 3.** Generated power by the PV plant

| Time | 8 a.m | 9 a.m | 10 a.m | 11 a.m | 12 p.m | 1 p.m | 2 p.m | 3 p.m | 4 p.m | 5 p.m |
|---|---|---|---|---|---|---|---|---|---|---|
| **Without STATCOM (kW)** | 108.5 | 262.2 | 345.9 | 422.5 | 465.1 | 463.7 | 429.4 | 333.4 | 203.3 | 51.41 |
| **With optimized STATCOM (kW)** | 125 | 298.5 | 431.4 | 528.9 | 581 | 579.7 | 536.8 | 418 | 254.7 | 62.93 |
| **Percentage of improvement** | 15.21 | 13.84 | 24.72 | 25.18 | 24.92 | 25.02 | 25.01 | 25.37 | 25.28 | 22.41 |

**TABLE 4.** Variable loads scenarios

| Scenario | Type | Value (P+ jQ) | Switching time |
|---|---|---|---|
| Load-A | Resistive-inductive | P=3.15 MW, Q=2.1 MVAR | from t=0 s to t=1 s |
| Load-B | Non-linear | P= 1.7 MW-4.7 MW, Q=0.8 MVAR-3.4 MVAR | from t=1 s to t=2 s |
| Load-C | Resistive-inductive | P=3.2 MW, Q=2.1 MVAR | from t=2 s to t=2.75 s |
| Load-D | Resistive | P=1.9 MW | from t=2.75 s to t=3.75 s |
| Load-E | Resistive-inductive | P=3.6 MW, Q=2.48 MVAR | from t=3.75 s to t=5.25 s |
| Load-F | Resistive-inductive | P=4.38 MW, Q=0.17 MVAR | from t=5.25 s to t=6 s |

**TABLE 5.** Impact of the optimized STATCOM on the power system during voltage sag fault

| | PCC voltage (pu) | $P_{pv}$ (MW) | $P_{wind}$ (MW) | $P_{hybrid}$ (MW) | $P_{load}$ (MW) | $Q_{load}$ (MVAR) |
|---|---|---|---|---|---|---|
| **Without STATCOM** | 0.5 | 0.79 | 2.19 | 2.98 | 0.74 | 0.84 |
| **With optimized STATCOM** | 0.67 | 1 | 2.86 | 3.83 | 1.32 | 1.51 |
| **Percentage of improvement** | 34% | 25.41% | 30.59% | 28.61% | 78.38% | 79.76 |

the STATCOM in enhancing the electrical utility operation is verified during different load scenarios and the occurrence of three-phase voltage sag in the grid. Based on the simulation results and discussions, the following points are noteworthy.

(a) When the optimized STATCOM is employed, the generated power from the hybrid system augments considerably by about 5.67%.
(b) The optimized STATCOM sustains the PCC voltage and the load voltage at the rated value (1 pu) irrespective of the load disturbances.
(c) Also, with the STATCOM support, the dynamic operation of the electrical grid is enhanced substantially by keeping always the grid power factor at unity.
(d) Moreover, with the utilization of the optimized STATCOM during the fault occurrence, the injected active and reactive power to the loads improves significantly by about 78.38% and 79.76%, respectively.

In our future work, the credibility of the proposed STATCOM system will be validated in other large-scale grid-connected systems including different Renewable Energy Sources (RES) and Fuel Cell (FC). Also, the effectiveness of the applied optimization algorithm will be evaluated in comparison with the latest optimization techniques such as the Grey Wolf Optimization (GWO) technique. In addition to that, we will be looking into using a wide range of data for the solar irradiance and the wind speed for many years or employing probabilistic modeling.

## NOMENCLATURE

| | |
|---|---|
| DFIG | Doubly Fed Induction Generator |
| GSC | Grid Side Converter |
| MPPT | Maximum Power Point Tracking |
| PCC | Point of Common Coupling |
| PSO | Particle Swarm Optimization |
| RSC | Rotor Side Converter |

STATCOM Static Synchronous Compensator

VSI Voltage Source Inverter

## References


[1] B. Jamil, A. T. Siddiqui, and N. Akhtar, "Estimation of solar radiation and optimum tilt angles for south-facing surfaces in Humid Subtropical Climatic Region of India," Engineering Science and Technology, an International Journal, vol. 19, pp. 1826-1835, 2016.

[2] V. Khare, S. Nema, and P. Baredar, "Solar–wind hybrid renewable energy system: A review," Renewable and Sustainable Energy Reviews, vol. 58, pp. 23-33, 2016.

[3] B. Sharma, R. Dahiya, and J. Nakka, "Effective grid connected power injection scheme using multilevel inverter based hybrid wind solar energy conversion system," Electric Power Systems Research, vol. 171, pp. 1-14, 2019.

[4] T. H. Rini and M. A. Razzak, "Voltage and power regulation in a solar-wind hybrid energy system," in IEEE International WIE Conference on Electrical and Computer Engineering (WIECON-ECE), pp. 231-234, 2015.

[5] D. Wu, G. S. Nariman, S. Q. Mohammed, Z. Shao, A. Rezvani, and S. Mohajeryami, "Modeling and simulation of novel dynamic control strategy for PV–wind hybrid power system using FGS− PID and RBFNSM methods," Soft Computing, pp. 1-23, 2019.

[6] K. Basaran, N. S. Cetin, and S. Borekci, "Energy management for on-grid and off-grid wind/PV and battery hybrid systems," IET Renewable Power Generation, vol. 11, pp. 642-649, 2016.

[7] J. Olamaei, S. Ebrahimi, and A. Moghassemi, "Compensation of voltage sag caused by partial shading in grid-connected PV system through the three-level SVM inverter," Sustainable Energy Technologies and Assessments, vol. 18, pp. 107-118, 2016.

[8] D. Lijie, L. Yang, and M. Yiqun, "Comparison of high capacity SVC and STATCOM in real power grid," in International Conference on Intelligent Computation Technology and Automation, pp. 993-997, 2010.

[9] E. Jamil, S. Hameed, and B. Jamil, "Power quality improvement of distribution system with photovoltaic and permanent magnet synchronous generator based renewable energy farm using static synchronous compensator," Sustainable Energy Technologies and Assessments, vol. 35, pp. 98-116, 2019.

[10] L. Kong, G. Cai, S. Xue, and S. Li, "Modeling and coordinated control strategy of large scale grid-connected wind/photovoltaic/energy storage hybrid energy conversion system," Mathematical Problems in Engineering, vol. 2015, pp. 1-15, 2015.

[11] J. R. Prabhakar and K. Ragavan, "STATCOM-based wind-solar-hydro electric power system with modified real and reactive power controls," International Journal of Emerging Electric Power Systems, vol. 15, pp. 45-58, 2014.

[12] A. M. Ibrahim, I. Hamdan, S. F. Al-Gahtani, H. S. Hussein, L. S. Nasrat, and M. A. Ismeil, "Optimal Shunt-Resonance Fault Current Limiter for Transient Stability Enhancement of a Grid-Connected Hybrid PV/Wind Power System," IEEE Access, vol. 9, pp. 126117 - 126134, 2021.

[13] K. D. Patlitzianas, "Solar energy in Egypt: Significant business opportunities," Renewable energy, vol. 36, pp. 2305-2311, 2011.

[14] M. El-Shimy, "Viability analysis of PV power plants in Egypt," Renewable energy, vol. 34, pp. 2187-2196, 2009.

[15] H. M. Sultan, O. N. Kuznetsov, and A. A. Z. Diab, "Site selection of large-scale grid-connected solar PV system in Egypt," in IEEE Conference of Russian Young Researchers in Electrical and Electronic Engineering (EIConRus), pp. 813-818, 2018.

[16] M. G. M. A. Y. Hatata, Rana M. Elmahdy, "Analysis of wind data and assessing wind energy potentiality for selected locations in Egypt," International Journal of Scientific & Engineering Research (IJSER), vol. 6, pp. 604-609, March-2015.

[17] O. Noureldeen, M. M. Youssef, and B. Hassanin, "Stability improvement of 200 MW Gabal El-Zayt wind farm connected to electrical grid using supercapacitor and static synchronous compensator during extreme gust," SN Applied Sciences, vol. 1, pp. 1-15, 2019.

[18] A. F. Tazay, A. M. Ibrahim, O. Noureldeen, and I. Hamdan, "Modeling, Control, and Performance Evaluation of Grid-Tied Hybrid PV/Wind Power Generation System: Case Study of Gabel El-Zeit Region, Egypt," vol. 8, pp. 96528- 96542, 2020.

[19] A. Fathy, "A reliable methodology based on mine blast optimization algorithm for optimal sizing of hybrid PV-wind-FC system for remote area in Egypt," Renewable energy, vol. 95, pp. 367-380, 2016.

[20] F. Diab, H. Lan, L. Zhang, and S. Ali, "An environmentally friendly factory in Egypt based on hybrid photovoltaic/wind/diesel/battery system," Journal of Cleaner Production, vol. 112, pp. 3884-3894, 2016.

[21] A. M. Abdelshafy, H. Hassan, A. M. Mohamed, G. El-Saady, and S. Ookawara, "Optimal grid connected hybrid energy system for Egyptian residential area," in international conference on sustainable energy engineering and application (icseea), pp. 52-60, 2017.

[22] Sanyo. Available at: <www.sanyo.co.jp/clean/solar/hit_e/download.html>.

[23] Gamesa, 2010. Gamesa G80-2.0 MW. Available online at<http://www.gamesacorp.com/files/File/G80-ingles.pdf>. Accessed on September 7, 2010.

[24] <https://www.google.com/maps>.

[25] <https://www.meteoblue.com>.

[26] A. Althobaiti, M. Armstrong, and M. Elgendy, "Current control of three-phase grid-connected PV inverters using adaptive PR controller," in 7th International Renewable Energy Congress (IREC), pp. 1-6, 2016.

[27] F. Hans, W. Schumacher, and L. Harnefors, "Small-signal modeling of three-phase synchronous reference frame phase-locked loops," IEEE Transactions on Power Electronics, vol. 33, pp. 5556-5560, 2017.

[28] A. Movahedi, A. H. Niasar, and G. Gharehpetian, "Designing SSSC, TCSC, and STATCOM controllers using AVURPSO, GSA, and GA for transient stability improvement of a multi-machine power system with PV and wind farms," International Journal of Electrical Power & Energy Systems, vol. 106, pp. 455-466, 2019.

[29] A. S. Al-Ogaili, I. B. Aris, R. Verayiah, A. Ramasamy, M. Marsadek, N. A. Rahmat, Y. Hoon, A. Aljanad, and A. N. Al-Masri, "A Three-Level Universal Electric Vehicle Charger Based on Voltage-Oriented Control and Pulse-Width Modulation," Energies, vol. 12, pp. 1-20, 2019.

[30] A. Parida and D. Chatterjee, "Cogeneration topology for wind energy conversion system using doubly-fed induction generator," IET Power Electronics, vol. 9, pp. 1406-1415, 2016.

[31] A. Parida and D. Chatterjee, "An improved control scheme for grid connected doubly fed induction generator considering

wind-solar hybrid system," International Journal of Electrical Power & Energy Systems, vol. 77, pp. 112-122, 2016.
[32] M. Chen, D. Fan, H. Fang, Y. Zhu, and P. Chen, "Control strategy of excitation converter in Doubly-Fed Induction Generator wind power generation system," in IEEE Conference on Energy Internet and Energy System Integration (EI2), pp. 1-5, 2017.
[33] J. Mohammadi, S. Vaez-Zadeh, E. Ebrahimzadeh, and F. Blaabjerg, "Combined control method for grid-side converter of doubly fed induction generator-based wind energy conversion systems," IET Renewable Power Generation, vol. 12, pp. 943-952, 2018.
[34] T. R. Ayodele, A.-G. A. Jimoh, J. Munda, and J. Agee, "Dynamic Response of a Wind Farm Consisting of Doubly-Fed Induction Generators to Network Disturbance," in Simulation and Modeling Methodologies, Technologies and Applications, ed: Springer, pp. 131-150, 2013.
[35] I. Hamdan, A. M. Ibrahim, and O. Noureldeen, "Modified STATCOM control strategy for fault ride-through capability enhancement of grid-connected PV/wind hybrid power system during voltage sag," SN Applied Sciences, vol. 2, pp. 1-19, 2020.
[36] M. I. Mosaad, H. S. M. Ramadan, M. Aljohani, M. F. El-Naggar, and S. S. Ghoneim, "Near-Optimal PI Controllers of STATCOM for Efficient Hybrid Renewable Power System," IEEE Access, vol. 9, pp. 34119-34130, 2021.
[37] A. Yahiaoui, F. Fodhil, K. Benmansour, M. Tadjine, and N. Cheggaga, "Grey wolf optimizer for optimal design of hybrid renewable energy system PV-Diesel Generator-Battery: Application to the case of Djanet city of Algeria," Solar Energy, vol. 158, pp. 941-951, 2017.
[38] A. M. Rauf and V. Khadkikar, "Integrated photovoltaic and dynamic voltage restorer system configuration," IEEE Transactions on Sustainable Energy, vol. 6, pp. 400-410, 2015.